



AFRL-AFOSR-VA-TR-2016-0319

Chirality-Controlled Growth of Single-Wall Carbon Nanotubes
Using Vapor Phase Epitaxy: Mechanistic Understanding and Scalable Production

Chongwu Zhou
UNIVERSITY OF SOUTHERN CALIFORNIA LOS ANGELES
UNIVERSITY GARDENS STE 203
LOS ANGELES, CA 90089-0001

09/15/2016
Final Report

DISTRIBUTION A: Distribution approved for public release.

Air Force Research Laboratory
AF Office Of Scientific Research (AFOSR)/RTB2

REPORT DOCUMENTATION PAGE
*Form Approved
OMB No. 0704-0188*

The public reporting burden for this collection of information is estimated to average 1 hour per response, including the time for reviewing instructions, searching existing data sources, gathering and maintaining the data needed, and completing and reviewing the collection of information. Send comments regarding this burden estimate or any other aspect of this collection of information, including suggestions for reducing the burden, to Department of Defense, Washington Headquarters Services, Directorate for Information Operations and Reports (0704-0188), 1215 Jefferson Davis Highway, Suite 1204, Arlington, VA 22202-4302. Respondents should be aware that notwithstanding any other provision of law, no person shall be subject to any penalty for failing to comply with a collection of information if it does not display a currently valid OMB control number.

PLEASE DO NOT RETURN YOUR FORM TO THE ABOVE ADDRESS.

1. REPORT DATE (DD-MM-YYYY) 15-06-2016	2. REPORT TYPE final	3. DATES COVERED (From - To) Jun 2014 - Jun 2016		
4. TITLE AND SUBTITLE Chirality-controlled growth of single-wall carbon nanotubes using vapor phase epitaxy: mechanistic understanding and scalable production		5a. CONTRACT NUMBER		
		5b. GRANT NUMBER FA9550-14-1-0115		
		5c. PROGRAM ELEMENT NUMBER		
6. AUTHOR(S) Zhou, Chongwu Zheng, Ming Liu, Bilu Liu, Jia Wu, Fanqi		5d. PROJECT NUMBER		
		5e. TASK NUMBER		
		5f. WORK UNIT NUMBER		
7. PERFORMING ORGANIZATION NAME(S) AND ADDRESS(ES) University of Southern California, Los Angeles, California 90089, United States National Institute of Standards and Technology, Gaithersburg, Maryland 20899, United States		8. PERFORMING ORGANIZATION REPORT NUMBER		
9. SPONSORING/MONITORING AGENCY NAME(S) AND ADDRESS(ES) Air Force Office of Scientific Research, Arlington, VA 22203		10. SPONSOR/MONITOR'S ACRONYM(S) AFOSR		
		11. SPONSOR/MONITOR'S REPORT NUMBER(S)		
12. DISTRIBUTION/AVAILABILITY STATEMENT Approved for Public Release; Distribution is Unlimited.				
13. SUPPLEMENTARY NOTES				
14. ABSTRACT In this report, we present our efforts in establishing a novel and effective approach for chirality-controlled synthesis of single-wall carbon nanotubes. Firstly, we have successfully demonstrated a vapor-phase-epitaxy-analogous general strategy for producing nanotubes of predefined chirality. By combining nanotube separation with synthesis, we have achieved controlled growth of nanotubes with preselected chirality. Moreover, we carried out systematic investigations of the chirality-dependent growth kinetics and termination mechanism for the vapor-phase epitaxial growth of seven different single-chirality nanotubes of (9, 1), (6, 5), (8, 3), (7, 6), (10, 2), (6, 6), and (7, 7), covering near zigzag, medium chiral angle, and near armchair semiconductors, as well as armchair metallic nanotubes. Furthermore, we explored and successfully managed to elongate organic synthesized (5, 5) end-cap molecules into small-diameter nearly-pure-semiconducting single-wall carbon nanotubes with vapor-phase-epitaxy cloning approach.				
15. SUBJECT TERMS Carbon nanotubes, chirality, vapor phase epitaxy, growth rate, lifetime, termination mechanism, semiconducting, end-cap molecules				
16. SECURITY CLASSIFICATION OF: a. REPORT b. ABSTRACT c. THIS PAGE		17. LIMITATION OF ABSTRACT UU	18. NUMBER OF PAGES 28	19a. NAME OF RESPONSIBLE PERSON Zhou, Chongwu 19b. TELEPHONE NUMBER (Include area code) (213)740-4708

AFOSR Final Performance Report
Chirality-Controlled Growth of Single-Wall Carbon Nanotubes
Using Vapor Phase Epitaxy: Mechanistic Understanding and Scalable Production

PI: Chongwu Zhou
University of Southern California
Co-PI: Ming Zheng
National Institute of Standards and Technology (NIST)

Introduction

Single-wall carbon nanotubes (SWCNTs) possess superior electrical and optical properties, and hold great promise for electronic and biomedical applications¹⁻¹⁰. As the electronic property of an SWCNT strongly depends on its chirality, the lack of synthetic control in chirality has long been recognized as a fundamental impediment in the science and application of SWCNTs. Previous efforts to address this issue have resulted in significant progress in separation of synthetic mixtures, yielding predominantly single-chirality nanotube species¹¹⁻¹⁵. However, separation processes are limited by their small scale, high cost and short length (<500 nm) of the resulting chirality-pure nanotubes. They are, therefore, not suitable for many, especially electronic device applications.

Realistic application of SWCNTs in electronic devices and integrated circuits requires that the electronic type of the nanotubes be well controlled. Selective synthesis of semiconducting or metallic predominated SWCNTs has already been achieved through controlled chemical vapor deposition (CVD) growth¹⁶⁻¹⁸, enabling the fabrication of nanotube field-effect transistors using predominantly semiconducting SWCNTs^{19, 20}. As a next step, synthesis of SWCNTs with predefined chirality is highly desired. However, this goal has remained elusive for some time in the nanotube field. For metal-catalyzed nanotube synthesis by CVD, it is generally believed that the diameters of the nanotubes are determined by the size of the catalytic metal particles. Unfortunately, attempts to control the size of the catalysts in hope of achieving chirality-controlled nanotube growth have not been successful²¹. Nanotube ‘cloning’ has been studied with^{22, 23} and without²⁴ metal catalyst particles showing various degree of success; however, controlled synthesis of nanotubes with predefined chiralities has not been achieved. In contrast, vapour-phase epitaxy

(VPE) such as molecular beam epitaxy and metal organic CVD has long been used by the semiconductor industry to grow two-dimensional epitaxial films, which can preserve the crystalline structure of the starting substrate. It is, therefore, very intriguing to explore the potential of using VPE for one-dimensional nanotube synthesis.

In this report, we present our efforts in establishing a novel and effective approach for chirality-controlled synthesis of SWCNTs. Firstly, we have successfully demonstrated a VPE-analogous general strategy for producing nanotubes of predefined chirality²⁵. By combining nanotube separation with synthesis, we have achieved controlled growth of nanotubes with preselected chirality. Moreover, we carried out systematic investigations of the chirality-dependent growth kinetics and termination mechanism for the vapor-phase epitaxial growth of seven different single-chirality nanotubes of (9, 1), (6, 5), (8, 3), (7, 6), (10, 2), (6, 6), and (7, 7), covering near zigzag, medium chiral angle, and near armchair semiconductors, as well as armchair metallic nanotubes²⁶. Furthermore, we explored and successfully managed to elongate organic synthesized (5, 5) end-cap molecules into small-diameter nearly-pure-semiconducting SWCNTs with VPE cloning approach²⁷. All the results presented in this report not only demonstrate a highly robust strategy, VPE cloning approach, to achieve chirality-predefined synthesis of SWCNTs, but also deepen our understanding of the chirality-dependent SWCNT growth kinetics and the underlying mechanism.

Chirality-controlled growth of SWCNTs using VPE cloning approach

In this section, we report our results of developing the VPE cloning approach for chirality pre-selected synthesis of SWCNTs²⁵. In our VPE cloning strategy, we combined nanotube separation with CVD synthesis together in order to achieve controlled growth of nanotubes with preselected chirality. Tremendous progress has been made in recent years in SWCNT separation^{11-15, 28, 29}. In particular, DNA-based chromatographic separation allows purification of both semiconducting and metallic single-chirality SWCNTs through the use of different DNA sequences^{12, 29}. In this work, three exemplary chirality-pure (7, 6), (6, 5) and (7, 7) SWCNT seeds with purity up to 90% are used. These serve as the starting templates for the ensuing catalyst-free, chirality controlled nanotube cloning process.

The schematic of the chirality-controlled SWCNT cloning process is illustrated in Fig. 1a. Firstly, chirality-pure SWCNT seeds obtained from the DNA-based separation were deposited onto the growth substrates using drop coating and incubation with different durations. The as-deposited seeds then went through an air and water vapour annealing process. This step removes the DNA wrapped on the nanotube seeds and activates the nanotube ends so that carbon reaction intermediates from decomposed feed stock can be efficiently added. Both methane and ethanol were found to be suitable as the carbon source to achieve chirality-controlled growth from these seeds.

We used atomic force microscopy (AFM) and scanning electron microscopy (SEM) to characterize SWCNTs before and after VPE cloning. Representative AFM images of (7, 6) SWCNT before and after cloning using ethanol on quartz substrates are presented in Fig. 1b. The average length of the nanotubes after cloning was measured to be $34.5 \pm 17.7 \text{ } \mu\text{m}$ (Fig. 1b), significantly longer than the average length of $0.34 \pm 0.15 \text{ } \mu\text{m}$ for the as-purified (7, 6) nanotube seeds (Fig. 1b). The measured diameter of the cloned nanotubes were approximately 0.9 nm, consistent with the (7, 6) nanotube diameter ($d=0.89 \text{ nm}$). As control experiments, blank quartz substrates and quartz substrates deposited with DNA solution but without any nanotube seeds were subjected to the air and water vapour annealing, and then the VPE cloning. No nanotube growth was observed after the VPE process. This demonstrates that the long SWCNTs were indeed grown from the nanotube seeds.

We show that purified single-chirality nanotube seeds of both semiconducting and metallic SWCNTs are significantly elongated through a catalyst-free VPE process, producing horizontally aligned SWCNT arrays on quartz substrates and randomly oriented SWCNTs on Si/SiO₂ substrates, with lengths more than tens of micrometres. Raman characterization confirms that the original chiralities of the nanotube seeds are preserved in the extended portion of the nanotubes, and the semiconducting nature of the grown (7, 6) and (6, 5) SWCNTs are further confirmed using electrical measurements on individual nanotubes.

Besides, we also carefully studied the effect of substrates on the VPE cloning process. On Si/SiO₂ substrates (Fig. 1c), random orientation was observed for the cloned nanotubes irrespective of the gas flow direction. For nanotube cloning performed on the ST-cut quartz substrates (Fig.

1d), the cloned SWCNTs were found to be horizontally aligned along the crystal orientation³⁰. This should be very useful for the fabrication of nanotube transistors and integrated circuits.

Overall, the nanotube VPE process was found to be very robust and highly reproducible. Various carbon feed stocks including methane and ethanol, and different nanotube seeds including (7, 6), (6, 5) and (7, 7) were used successfully. The SEM image of (7, 6) nanotubes cloned with methane (Fig. 1e) and ethanol (Fig. 1c and Fig. 1d) indicate that similar growth were achieved for different carbon sources.

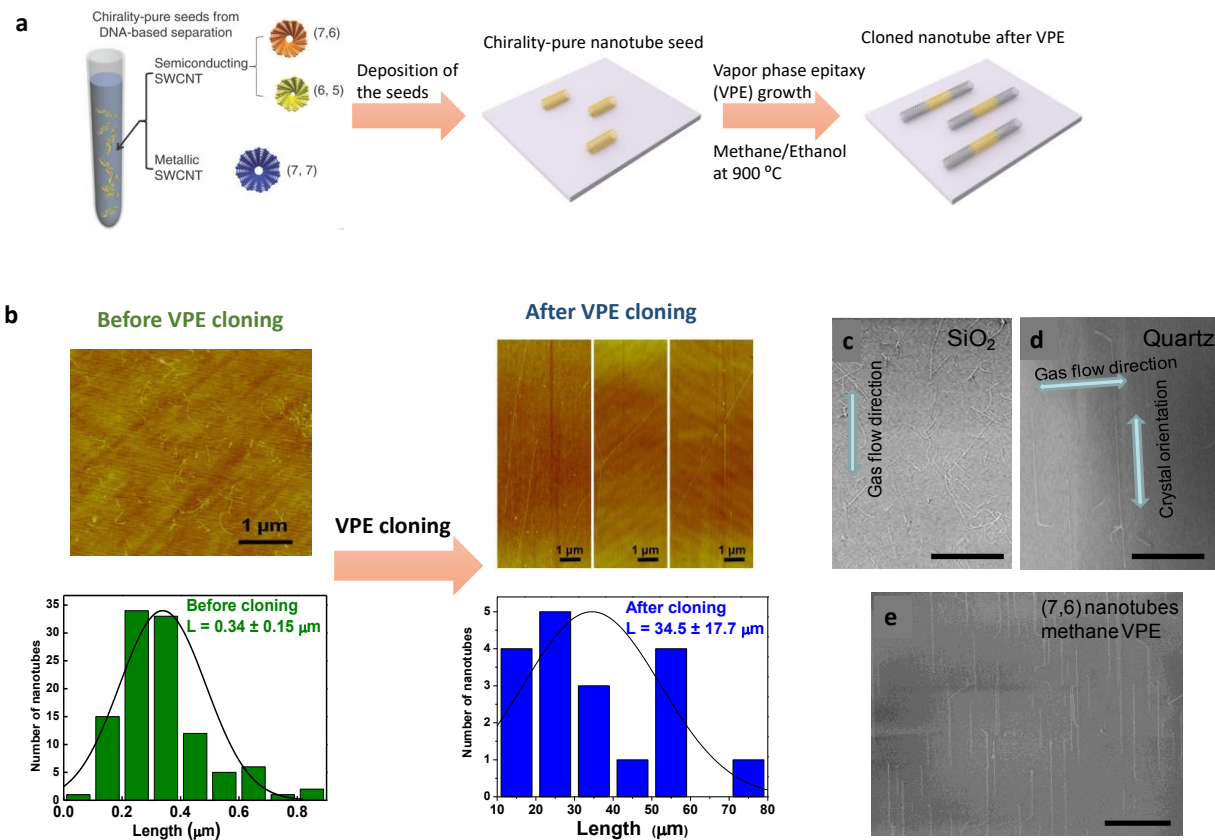


Figure 1. (a) Schematic illustration of the VPE process for chirality controlled SWCNT synthesis. (b) AFM images and length distribution of the (7, 6) nanotubes before and after VPE using ethanol on quartz substrates. (c,d) Comparison of (7, 6) nanotubes cloned on quartz (d) and Si/SiO₂ (c) substrates. (e) An SEM image showing (7, 6) nanotubes cloned on the quartz substrate using methane. Scales bars, 50 μm for (c,d), 30 μm for (e).

In order to determine whether the original chiralities were preserved during the cloning process, we used micro-Raman to characterize the pristine and cloned SWCNTs. For the (7, 6) case, we used 1.96 eV laser excitation, which is close to the second optical transition $E_{22}=1.92$ eV of the (7,

6) nanotubes³¹. To further enhance the signal-to-noise ratio, surface-enhanced Raman spectroscopy was used after e-beam evaporation of 5 nm silver on the substrate. The radial breathing mode (RBM) Raman spectra taken at different random locations on the substrates before and after cloning are presented in Fig. 2a,b, respectively. For small diameter nanotubes such as (7, 6), (6, 5) and (7, 7), adjacent nanotubes have very distinct RBM frequencies (Fig. 2f)³², allowing unambiguous chirality assignment by determining the RBM frequency and the laser excitation energy. Fig. 2a,b show predominant peaks at 265 cm⁻¹, which correspond to the RBM of (7, 6) nanotubes, indicating that the chirality is indeed preserved in the cloned nanotubes. The minority peaks at 300 and 307 cm⁻¹ can be attributed to the (8, 3) and (9, 1) impurities. We have also performed Raman mapping along a specific nanotube as shown in Fig. 2c, confirming that the chirality is preserved along the whole nanotube. Similar studies were carried out for (7, 7) nanotubes using 2.4 eV laser excitation; Raman spectra of (7, 7) before (Fig. 2d) and after VPE growth (Fig. 2e) showed predominant peaks at 249 cm⁻¹, which correspond to the RBM of (7, 7) nanotubes. The weak peak at 303 cm⁻¹ is attributed to the Si/SiO₂ substrate background. The RBM intensity of cloned nanotubes is weaker than that of the nanotube seeds. This is because many nanotube seeds got etched away during the annealing and subsequent VPE step, thus leading to reduced nanotube number density and reduced Raman intensity.

Back-gated nanotube field-effect transistors were fabricated to further characterize the electrical properties of the cloned (7, 6) and (6, 5) nanotubes. The device schematic and an SEM image of a representative device consisting of an individual (7, 6) nanotube are shown in Fig. 2g,h, respectively. In brief, the cloned (7, 6) nanotubes grown on quartz substrates were transferred to Si/SiO₂ substrates with 50nm SiO₂ using methods described in our previous publication⁹. This was followed by formation of Ti/Pd (0.5/50 nm) source/drain metal contacts using lithography and lift-off techniques. After production, the device had a channel length of L=4 μ m and a 50-nm-thick SiO₂ gate dielectric. The transfer characteristics (I_D – V_G) measured at various V_D biases, shown in Fig. 2i, clearly indicate that the device is made of a semiconducting nanotube. This is consistent with the (7, 6) chirality. We measured a total of 17 such devices produced with individual cloned (7, 6) nanotubes and found that all of them exhibit similar semiconducting behavior. Similar electrical characteristics were also observed for transistors made from cloned (6, 5) nanotubes. These electrical measurements further confirm that chirality-controlled cloning was achieved and, moreover, demonstrate the preservation of superior electrical properties in the cloned nanotubes.

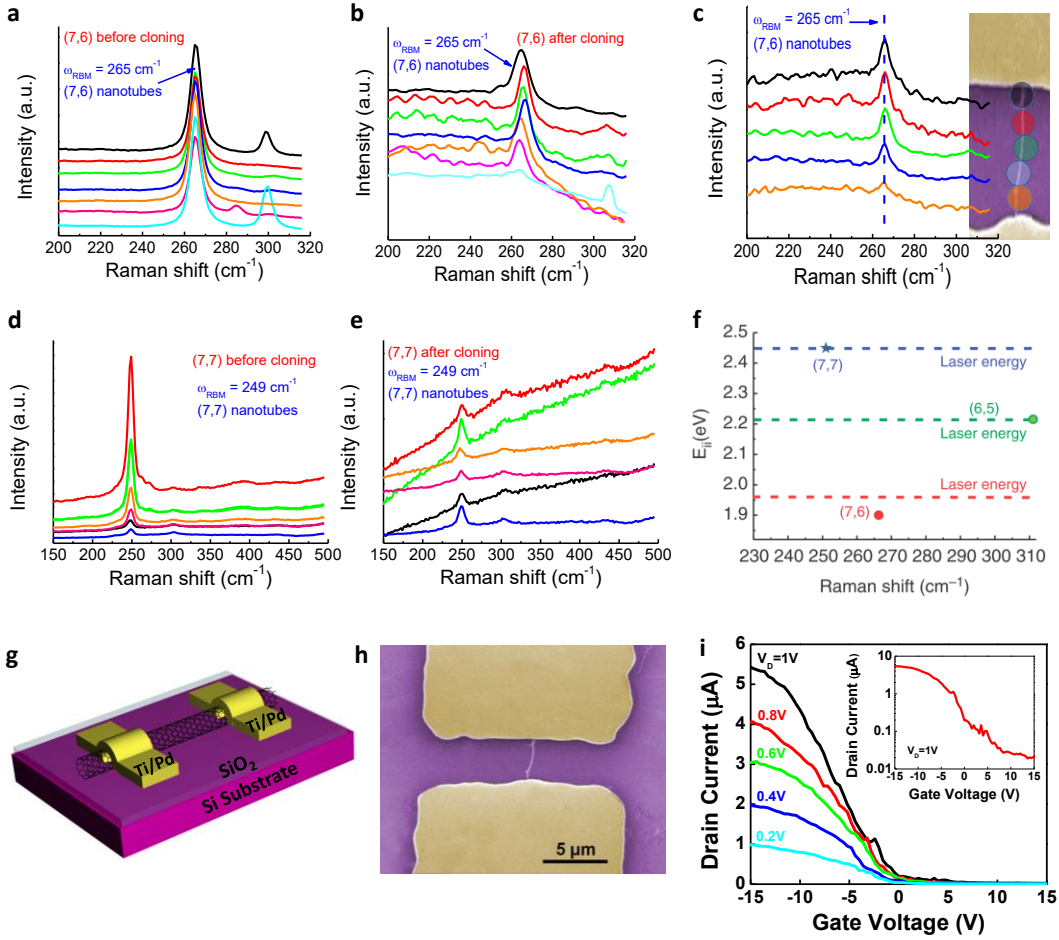


Figure 2. (a,b) Raman RBMs of (7, 6) nanotubes before and after VPE. The spectra were taken at different random locations on the quartz substrates with laser excitation energy of 1.96 eV. The peaks at 265 cm^{-1} correspond to the RBM of (7, 6) nanotubes. (c) Raman RBM spectra along a specific nanotube confirming that the chirality is preserved after the VPE process. Inset, an SEM image (with artificial colour) of the nanotube. (d,e) Raman RBMs of (7, 7) nanotubes before and after VPE. The spectra were taken at different random locations on the Si/SiO₂ substrates with laser excitation energy of 2.4 eV. The peaks at 249 cm^{-1} correspond to the RBM of (7, 7) nanotubes. (f) Kataura plot shows the RBM frequencies and E_{ii} of different nanotubes. The values were taken from the literature³². (g) Schematic and (h) an SEM image (with artificial colour) of a back-gated (7, 6) nanotube transistor. The device consists of an individual (7, 6) nanotube, with $L=4\text{ }\mu\text{m}$ and 50 nm thick SiO₂ gate dielectric. (i) Transfer characteristics (I_D - V_G) of the transistor measured at various V_D biases. Inset, transfer characteristics plotted in semi-logarithm scale with $V_D=1\text{ V}$.

What is the mechanism of the VPE-based SWCNT cloning? We attempt to explain the growth mechanism by proposing a molecular model. We emphasize the tentative nature of this model and present it in the spirit of stimulating further exploration of the VPE-based SWCNT cloning. We find that annealing is a critical step for successful SWCNT cloning. The edges of purified SWCNT seeds are created by the sonication process for dispersion. Cavitation ruptures C–C bonds, most

likely leading to oxidation of carbons at the cutting edges to form $-\text{COOH}$, or reconstruction of carbons at the edges to form 5- or 7-membered ring structures, making the edges not suitable for continued growth. Air oxidation and subsequent hydrogen and water treatment most likely remove these defective carbons and expose more reactive hydrogen-terminated sp^2 carbon edges for growth (Fig. 3a). We believe the essence of SWCNT cloning by VPE is to incorporate certain pyrolysis products into a graphitic carbon structure defined by the purified SWCNT seed. We propose that this is achieved by covalent addition of C_2H_2 and C_2H_4 at the SWCNT edge. More specifically, we propose that the chemistry between $\text{C}_2\text{H}_2/\text{C}_2\text{H}_4$ and SWCNT edge follows the classic organic chemistry reaction for the generation of six-membered rings: Diels–Alder cycloaddition. As shown in Fig. 3b, acetylene C_2H_2 can be incorporated into a site with armchair configuration through the Diels–Alder reaction (reaction 1), followed by a re-aromatization step (reaction 2). Similar reactions between C_2H_2 and polycyclic aromatic hydrocarbons in organic solvents have been recently shown and proposed as the basis for metal-catalyst-free synthesis of SWCNTs by Fort et al.^{33, 34} Likewise, C_2H_4 can also be incorporated into an armchair site through the Diels–Alder reaction (reaction 3). The C–C single bond created by reaction 3 can be converted into a double bond via a radical ($\text{CH}_3\cdot$ or $\text{H}\cdot$)-catalysed step (reaction 4). In both cases, the final product is a new six-membered sp^2 carbon ring built on the SWCNT edge. The whole process can be repeated at other existing or newly built armchair sites, resulting in elongation of the SWCNT with conservation of chirality defined by the seed. Growth termination may occur as a result of edge reactions with other reactive pyrolysis products.

The Diels–Alder chemistry in the cloning mechanism requires the presence of armchair sites on the SWCNT edge. A natural consequence of this requirement is chirality-dependent growth rate. In general, for a (n, m) tube there are m armchair sites at the edge, and the rate of carbon incorporation should be proportional to m . The rate of tube length elongation R can be obtained after normalizing the rate of carbon incorporation by the tube circumference:

$$R \propto \frac{m}{\sqrt{n^2 + nm + m^2}} \quad (1)$$

Fig. 3c illustrates the end edges of two semiconducting tubes of the same diameter $(6, 5)$ and $(9, 1)$, unzipped along the tube axis. According to the above analysis, $(6, 5)$ tubes should grow five times faster than $(9, 1)$. In the next section of this report, we present our results of the systematic investigations of chirality-dependent growth kinetics and termination mechanisms of 7 different single-chirality nanotubes, $(9, 1)$, $(6, 5)$, $(8, 3)$, $(7, 6)$, $(10, 2)$, $(6, 6)$, and $(7, 7)$, covering near

zigzag, medium chiral angle, and near armchair semiconductors, as well as armchair metallic nanotubes.

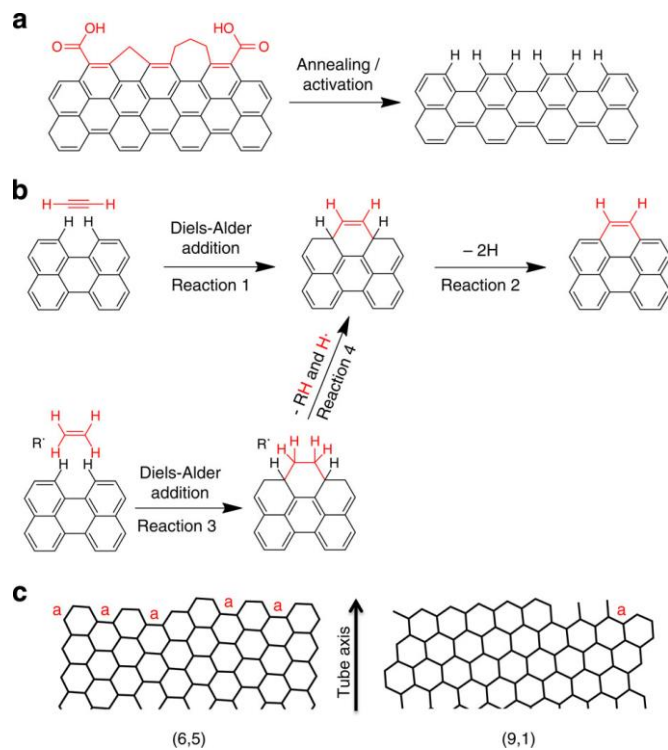


Figure 3. Molecular mechanism of SWCNT cloning via VPE. (a) The effect of annealing. (b) Diels–Alder chemistry for the incorporation of C₂H₂ and C₂H₄ into an armchair site on the edge of a growing SWCNT seed. (c) Edge structures of unzipped ((6, 5) and (9, 1)) tubes. The red letter “a” denotes an armchair site on the edges.

In conclusion, we have demonstrated that chirality-controlled SWCNT growth can be achieved using catalyst-free VPE growth, which produces single-chirality, horizontally aligned nanotubes with significantly longer lengths than the as-purified seeds. Although this work only focused on the semiconducting (7, 6), (6, 5) and metallic (7, 7) nanotube species, we believe that the cloning process described here should be applicable to other semiconducting and metallic chiralities²⁹. Our cloning method therefore opens up a possibility to study catalyst-free nanotube VPE growth mechanism as a function of chirality. With its versatility and reproducibility, the cloning technology platform should greatly benefit the device and circuit application of nanotubes. Moreover, future research on improving the cloning yield, density and precise positioning of the nanotube seeds could potentially lead to the long-dreamed, integrated functional “carbon-only” electronic systems.

Chirality-dependent VPE growth kinetics and termination mechanism

In this section, we report our progress in chirality-dependent growth kinetics and termination mechanism for the vapor-phase epitaxial growth of seven different single-chirality nanotubes of (9, 1), (6, 5), (8, 3), (7, 6), (10, 2), (6, 6), and (7, 7), covering near zigzag, medium chiral angle, and near armchair semiconductors, as well as armchair metallic nanotubes²⁶. Our results reveal that the growth rates of nanotubes increase with their chiral angles while the active lifetimes of the growth hold opposite trend. Consequently, the chirality distribution of a nanotube ensemble is jointly determined by both growth rates and lifetimes. These results correlate nanotube structures and properties with their growth behaviors and deepen our understanding of chirality-controlled growth of nanotubes.

The VPE-based cloning process follows the method we previously reported²⁵ with some improvements. A small amount (optimized at 10 sccm) of C₂H₄ was added into VPE process and the SEM characterization showed the yield of SWCNTs improved significantly with optimal amount of C₂H₄ addition. This yield improvement paves the way for the study of chirality-dependent growth and termination of large amount of SWCNTs. Fig. 4a shows the chirality map of seven kinds of nanotubes we studied in this work. The three important structural and property parameters of SWCNTs, that is, chiral angle, diameter, and metallicity, are highlighted. As an illustration, Fig. 4b compares the edge structures of (9, 1) and (6, 5) SWCNTs, where the differences in their edge-atom configurations can be clearly discerned. One important question here is how the edge structures of nanotubes influence their growth behaviors.

To obtain information on the growth kinetics of SWCNTs, we performed systematical experiments at different growth times ranging from tens of seconds to 15 min. Fig. 4c–e presents SEM images of (9, 1) SWCNTs with growth duration of 40 s, 60 s, and 15 min, respectively. The average nanotube length (\bar{L}) for each duration was measured and presented in Fig. 4i, which demonstrates that the length of (9, 1) nanotubes keep growing during this period of time. As a comparison, Fig. 4f–h shows the SEM images of (6, 5) SWCNTs with growth time of 20 s, 40 s, and 15 min, with the length distribution histogram shown in Fig. 4j. In sharp contrast to (9, 1) nanotubes, we found that the (6, 5) nanotubes have nearly the same average lengths with different growth periods, suggesting the active growth lifetime is very short. Note that both (9, 1) and (6, 5)

nanotubes are the semiconducting type with identical diameters but distinct chiral angles. Specifically, (6, 5) is a near-armchair SWCNT with a chiral angle of 27.0 °, while (9, 1) represents a near-zigzag SWCNT with a chiral angle of only 5.2 °. This result clearly demonstrates the influence of chiral angles on the growth of SWCNTs.

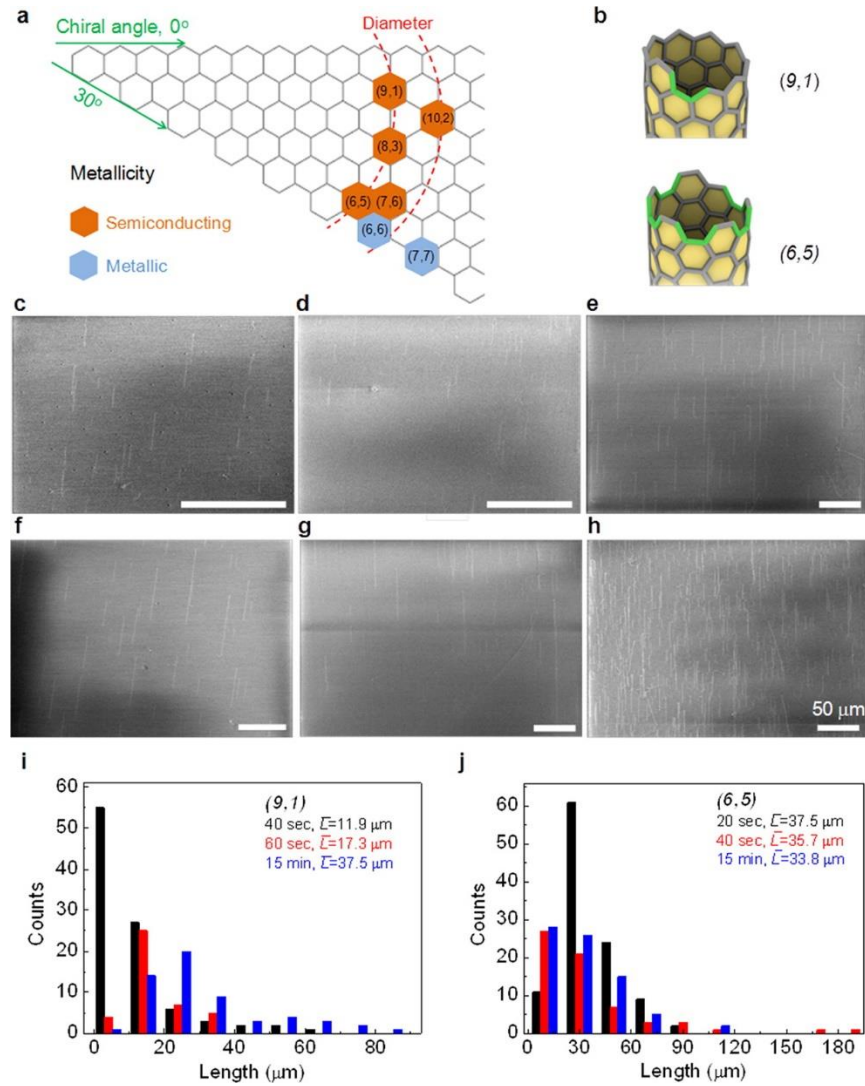


Figure 4. Chirality-dependent growth and length distribution of semiconducting (9, 1) and (6, 5) SWCNTs. (a) Chirality map and chiral angle, diameter, and metallicity information of seven nanotubes we studied. (b) Edge structure comparisons of (9, 1) and (6, 5) nanotubes. (c–e) SEM images of VPE-grown (9, 1) SWCNTs with growth time of 40 s, 60 s, and 15 min, respectively. (f–h) SEM images of VPE-grown (6, 5) SWCNTs with growth time of 20 s, 40 s, and 15 min, respectively. (i,j) Length distribution of nanotubes from (c–e) and (f–h), respectively. Scale bars are 50 μm for all images.

To get in depth and comprehensive information on the growth kinetics, we systematically studied the growth of five types of semiconducting SWCNTs under various growth times, that is, 20, 30, 40, 60, 120, and 900 s. Colored dots in Fig. 5a show the length evolutions of these five nanotubes. It is evident that these nanotubes possess distinct growth kinetics, especially during the initial growth period, as shown in Fig. 5b. To quantitatively analyze the nanotube growth kinetics and to model the growth process that has a finite period, that is, growth plus termination, we assume the average growth rate (\bar{R}_t) of a (n, m) SWCNT at time t follows exponential kinetics

$$\bar{R}_t = \bar{R}_0 \exp\left(-\frac{t}{\tau}\right) \quad (2)$$

Here, \bar{R}_0 and τ are the average initial growth rate and lifetime for a SWCNT. Consequently, the average nanotube length (\bar{L}_t) at time t would be

$$\bar{L}_t = \int_0^t \bar{R}_t dt = \bar{R}_0 \tau \cdot \left[1 - \exp\left(-\frac{t}{\tau}\right)\right] \quad (3)$$

Then, equation 3 was used to fit the length evolution profiles of the preceding mentioned five SWCNTs (solid curves in Fig. 5a) and extracted the two parameters, that is, \bar{R}_0 and τ for each nanotube. Here we emphasize that the nanotubes we studied fall into two subgroups with very similar diameters in each subgroup (inset of Fig. 5a), thus excluding any effect of nanotube diameter on their growth kinetics.^{14, 35, 36} Since all five of these nanotubes are semiconducting ones, the only noticeable structural parameter difference within each subgroup is the chiral angle. Therefore, the above results suggest a clear chiral angle-dependent growth behavior of SWCNTs.

We further plotted chiral angle versus growth rate and lifetime for these five SWCNT chirality species in Fig. 5c,d. As can be clearly discerned from Fig. 5c, nanotube growth rate increases with increasing its chiral angle, a result similar to that of a very recent report on metal catalyst driven CVD grown nanotubes.³⁷ Here we note that for VPE-cloning process, both ends of the seed from metal-catalyzed CVD processes where only catalyst nanotube joint point is active. Consequently, the actual growth rate of each (n, m) SWCNT may be over established by a factor of 2. Nevertheless, this will not have any influence on the trend of chirality-dependent growth rate of SWCNTs we have concluded. In addition to the chirality-dependent growth rates of nanotubes, more interestingly, we observed an opposite trend for chiral angle dependent lifetimes, that is, the lifetime of a nanotube decreases while increasing its chiral angle (Fig. 5d). Specifically, both (9, 1) and (10, 2) nanotubes possess lifetimes of ~ 80 s under our growth condition, which are much longer than (8, 3) nanotube with a lifetime of ~ 40 s and (6, 5) and (7, 6) nanotubes with a lifetime

of less than 20 s. Therefore, we emphasize that the final product distribution of a SWCNT ensemble neither solely relies on their growth rates nor their active lifetime as understood previously, but on their product $\bar{R}_0 \times \tau$.

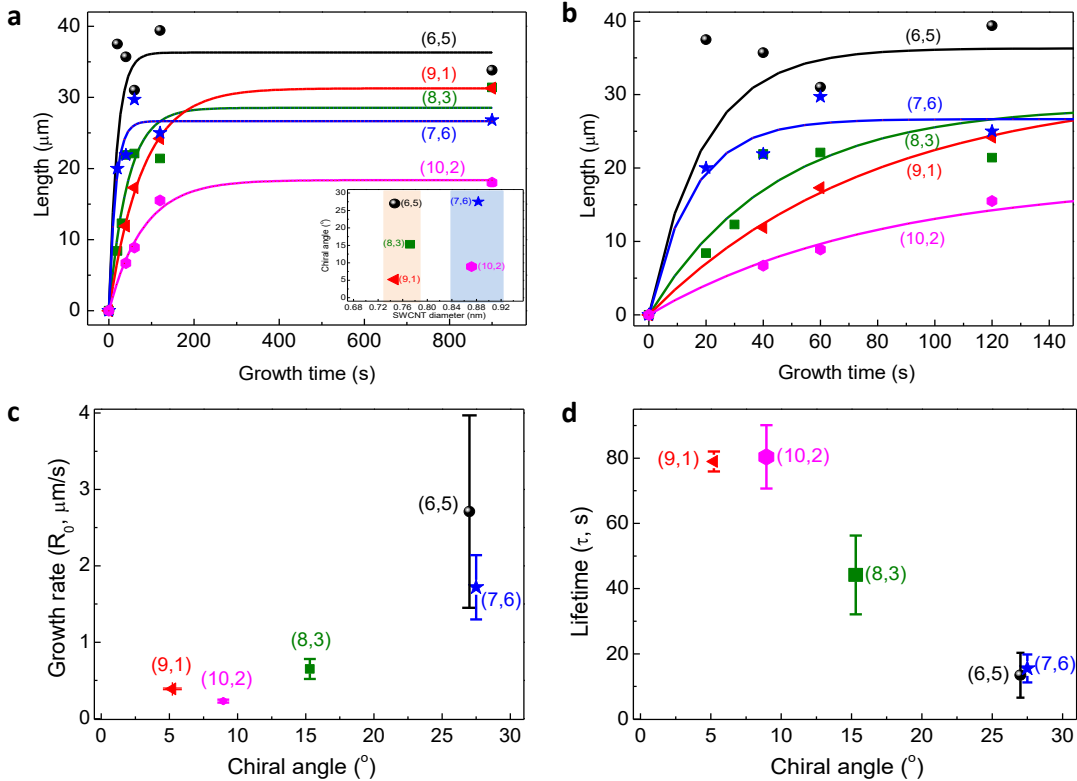


Figure 5. Length evolution profiles and chirality-dependent growth rate (R_0) and lifetime (τ) of semiconducting SWCNTs. (a) Length evolution profiles and fitted curves based on eq 3 for (6, 5), (8, 3), (9, 1), (7, 6), and (10, 2) SWCNTs with growth times of 20 s, 40 s, 60 s, 2 min, and 15 min. Inset, chiral angle versus diameter for the above five semiconducting SWCNTs, showing that they belong to two subgroups with similar diameters in each one as highlighted by different colors. (b) Zoom-in plot of panel a shows the initial growth period. (c,d) Chiral-angle-dependent growth rate (R_0) and lifetime (τ) of the above five kinds of semiconducting SWCNTs. The vertical error bars in c and d correspond to the errors of parameters extracted based on eq 3.

We propose that the above chirality-dependent growth rate and lifetime phenomena can be interpreted in the framework of Diels–Alder cycloaddition mechanism.^{25, 33, 38} According to the Diels–Alder chemistry, active carbon species will only be added to the armchair sites (serve as dienophile) on the open edges of SWCNTs during VPE-based cloning process.²⁵ Note that a particular (n, m) SWCNT has a total of m armchair sites (Fig. 6a,e), which can simultaneously accept coming carbon species for nanotube growth (Fig. 6a–c and Fig. 6e–g). Therefore, it is a

natural consequence that nanotubes with large m possess high growth rate. In real nanotube growth process, however, the situation may not be that ideal and we speculate that each adding step has a certain failure possibility. Previous studies on CH_4 pyrolysis show that it follows the sequence of $\text{CH}_4 \rightarrow \text{CH}_3 \rightarrow \text{C}_2\text{H}_6 \rightarrow \text{C}_2\text{H}_4 \rightarrow \text{C}_2\text{H}_2 \rightarrow \dots \rightarrow \text{C}$ (solid) at temperature of ~ 900 $^{\circ}\text{C}$.³⁹ Apparently, there exist various CH_x , C_2H_x , and even C_3H_x species in the CVD environment.⁴⁰ We note that the addition of CH_x or C_3H_x species instead of C_2H_x will generate five- or seven-membered ring on nanotubes (Fig. 6d,h), which in turn may prevent further nanotube growth via Diels-Alder chemistry. On the basis of recent theoretical studies,^{38, 41} the formation of six-membered ring is more energetically favorable than other kinds of structures especially when the nanotube segment is long. Nevertheless, there is still a very low but certain possibility for five- or seven-membered ring formation, which in turn will terminate nanotube growth. We emphasize that for nanotubes with large m , the adding events would happen more frequently than those nanotubes with small m . Consequently, it will take much shorter time for these larger m nanotubes to form the five- or seven-membered rings than the smaller m ones from statistical point of view, suggesting a shorter lifetime for nanotubes with larger m . Note that this does not necessarily mean lifetime is directly proportional to $1/m$, as the nanotube diameter may also play a role on its growth^{36, 38}. Nevertheless, it is safe to conclude, based on the Diels–Alder process illustrated in Fig. 6, that SWCNTs with larger m would have higher growth rates and shorter active lifetimes. This conclusion agrees very well with our experimental observations as for nanotubes with similar diameters, large chiral angle corresponds to large m . Importantly, we note that a screw dislocation mechanism has been experimentally identified for catalyst-free growth of nanowires in CVD process,⁴² which resembles the VPE growth of nanotube via Diels–Alder mechanism, especially for $(n, 1)$ nanotubes. Consequently, the results in this study connect nanotubes with nanowires and indicate that there might be a general growth mechanism for one-dimensional crystalline nanostructures. The chirality-dependent growth behavior and termination mechanism, however, is not reflected by nanowire growth case. Therefore, the results from this study provide new insight on the controlled growth of one-dimensional nanostructures and materials.

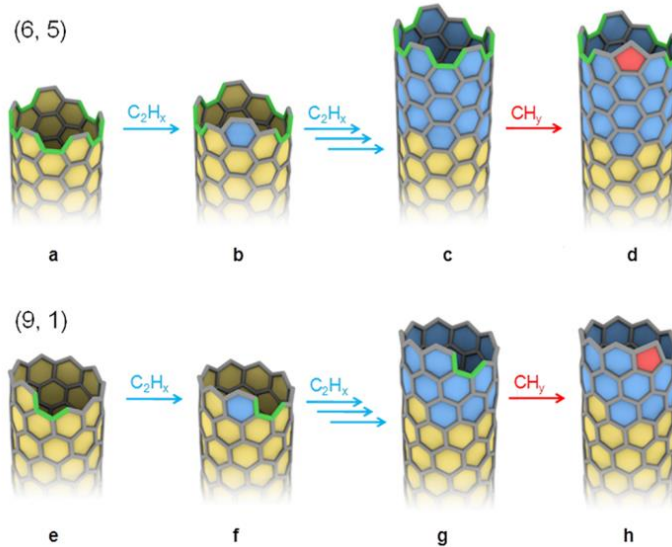


Figure 6. Atomic illustration of chirality-dependent SWCNT growth via Diels–Alders cycloaddition processes. (a–c) Cycloaddition of C_2H_x species to a (6, 5) SWCNT and the formation of six-membered rings, leading to the continuous growth of this nanotube. (d) Addition of CH_y species leads to the formation of five-membered ring and consequently nanotube growth stops. (e–g) Addition of C_2H_x species to a (9, 1) SWCNT for its continuous growth. (h) Addition of CH_y species leads to the growth stops. Multiple arrows from panels b to c and panels f to g represent multiple addition reactions.

Among all kinds of SWCNTs, armchair (n, n) nanotubes are of particular interest since they are the only true metallic nanotubes with zero band gap and linear energy dispersion relationships at Dirac point.⁴³ Our DNA-based separation method is capable of purifying such armchair metallic nanotubes, for example, (6, 6) and (7, 7), with high purity.²⁹ Here, we chose these two kinds of armchair nanotubes and studied their growth kinetics. Showing in Fig. 7a,b are the SEM images of the (6, 6) and (7, 7) SWCNTs with a growth time of 20 s. Surprisingly, we found that both nanotubes have relatively short average length (11.5 μm for (6, 6) and 6.4 μm for (7, 7)). We further studied the length evolution of these two armchair SWCNTs with growth time of 40 and 60 s (Supporting Information of ref²⁶). As shown in Fig. 7c,d, both nanotubes stop growth within 20 s, indicating a very short lifetime, which is consistent with our experimental observations and Diels–Alder cycloaddition mechanism proposed on large chiral angle SWCNTs. While it is difficult to accurately calculate the growth rate for these two nanotubes since they saturated within the shortest experimental time, we would like to comment on their saturated lengths and compare with their semiconducting counterparts, for example, (6, 6) versus (6, 5). The most noticeable difference is that (6, 6) nanotubes possess much shorter, $\sim 1/3$, saturated length as compared with (6, 5) ones, which has never been reported before. One interesting phenomenon we noted is that

in real SWCNT samples, armchair ones abnormally do not occupy a large population based on the electron diffraction analysis.⁴⁴ This result is consistent with our observation here shown that armchair nanotubes possess shorter saturated lengths than other nanotubes, that is, they are less abundant in a nanotube ensemble. We noticed that armchair nanotubes are the only true metallic ones with zero bandgap, thus it is intriguing to study whether the electronic properties of nanotubes have a strong effect on the growth. Further experiments that can well control the growth period into a very short time, for example, a few seconds,³⁵ combined with theoretical simulations, may help to understand the abnormal behavior of armchair SWCNTs, which may open up a novel window to exploring metallic/semiconducting controlled synthesis. Furthermore, future comparative studies of non-armchair metallic SWCNTs (e.g., semi-metallic SWCNTs), armchair metallic SWCNTs, and semiconducting ones would be important to further determine possible effect of metallicity on the growth of nanotubes, which could not be done at this moment due to lack of chirality-pure non-armchair metallic SWCNT seeds.

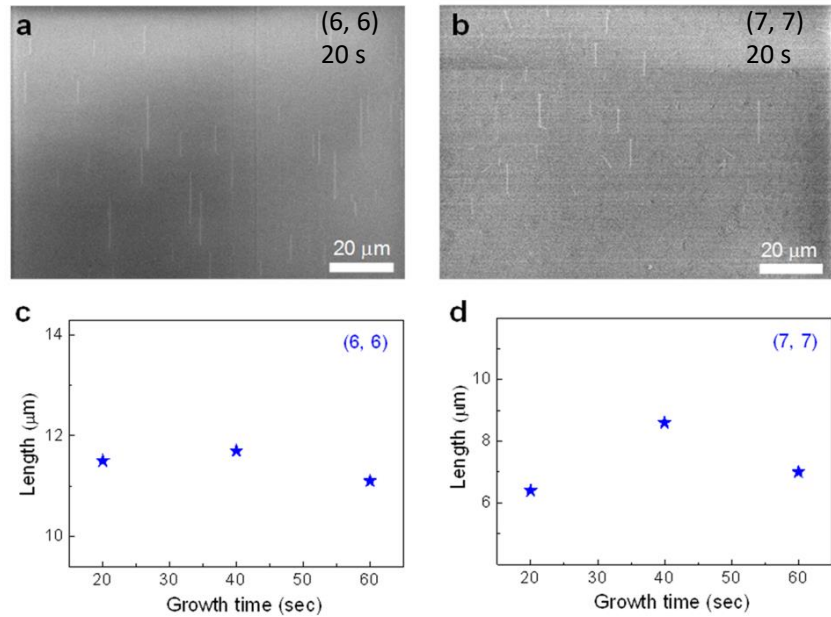


Figure 7. Chirality-dependent growth of armchair metallic SWCNTs. (a,b) Representative SEM images of cloned (6, 6) and (7, 7) SWCNTs with a growth time of 20 s. (c,d) Length evolution of (6, 6) and (7, 7) SWCNTs with growth time of 20, 40, and 60 s.

In conclusion, we systematically studied the chirality-dependent growth rate and active lifetime of both semiconducting and metallic SWCNTs in a recently established VPE-based cloning platform. Our research reveals distinct growth behaviors among SWCNTs and correlate with their structures within the framework of Diels–Alder chemistry. The abnormal growth behavior of

armchair nanotubes suggests a possible correlation between nanotube growth and their electronic characteristics. This work provides direct experimental evidence on the chirality-dependent growth kinetics of single-chirality nanotubes, which can guide further synthetic processes designed toward chirality-pure SWCNT synthesis.

VPE cloning of molecular end-caps

Recently, there has been increasing interest in using structurally well-defined carbon nanomaterials^{22, 24-26, 33, 45-49} to initiate nanotube growth with an aim of producing uniform SWCNTs. As is shown in the previous two sections of this report, our VPE cloning approach has successfully realized chirality pre-defined synthesis of 7 different single-chirality SWCNTs. However, the yield of the cloning process is still rather low at the current stage, largely due to very low areal number densities of nanotube seeds. In this section, we report a new nanotube growth method that combines bottom-up organic chemistry synthesis with VPE cloning approach^{25, 26} to achieve metal-catalyst-free growth of nearly-pure-semiconducting SWCNTs and their aligned arrays²⁷.

We started with the corannulene molecule ($C_{20}H_{10}$, structure shown in Fig. 8a) for the synthesis of the end-caps of nanotubes ($C_{50}H_{10}$, structure shown in Fig. 8b), aiming at chirality-controlled growth of SWCNTs via molecular cap engineering. The synthesis details of end-caps is presented in method section of ref²⁷. We point out metal elements such as Fe, Co, Ni, Cu, and so forth, which can act as catalysts for CVD growth of nanotubes, were not used in the above organic chemistry synthesis process. Therefore, it is safe to conclude that the as-formed $C_{50}H_{10}$ molecules are free of such metals, as confirmed using the energy dispersive X-ray (EDX) characterization. The as-synthesized red-orange powder of $C_{50}H_{10}$ was first dissolved in toluene to make a stable solution (Fig. 8d). Then, the quartz substrates with $C_{50}H_{10}$ molecules were subjected to a horizontal CVD furnace for subsequent nanotube growth. We initially conducted nanotube growth experiments without any pretreatment of $C_{50}H_{10}$. However, no nanotubes grew under broad growth conditions. Then, we reexamined the whole process and considered the possibility that the rims of the $C_{50}H_{10}$ molecules might be covered by other $C_{50}H_{10}$ molecules or solvents, embedding the active edges inside larger aggregates, as supported by the AFM characterization. Faced with this conjecture, we speculated that pretreatment might be necessary to initiate nanotube growth from this molecular

end-cap. After extensive exploration, ultimately we found that high-temperature air treatment, followed by water vapor treatment, is very effective in activating $C_{50}H_{10}$ for nanotube growth. In particular, we learned that air oxidation at 500 °C followed by water vapor treatment at 900 °C gives the highest nanotube yield (Fig. 8e).

We used SEM to examine the overall growth efficiency of nanotubes from pretreated $C_{50}H_{10}$. High magnification SEM characterization (Fig. 8e) clearly shows highly efficient growth of dense SWCNTs on quartz substrate. The yield of SWCNTs grown from $C_{50}H_{10}$ is much higher than that grown from short nanotube seeds, because the area number density of small $C_{50}H_{10}$ molecules is significantly larger than the area number density of nanotube seeds. As control experiments, we performed nanotube synthesis experiments using blank quartz substrates, following the identical air and water pretreatment, and no SWCNTs growth was observed. Overall, the above experiments unambiguously demonstrate that nanotube growth is indeed initiated by the deposited $C_{50}H_{10}$ molecules. We used AFM to study the diameters of the as-grown SWCNTs and found that most nanotubes have heights below 1nm.

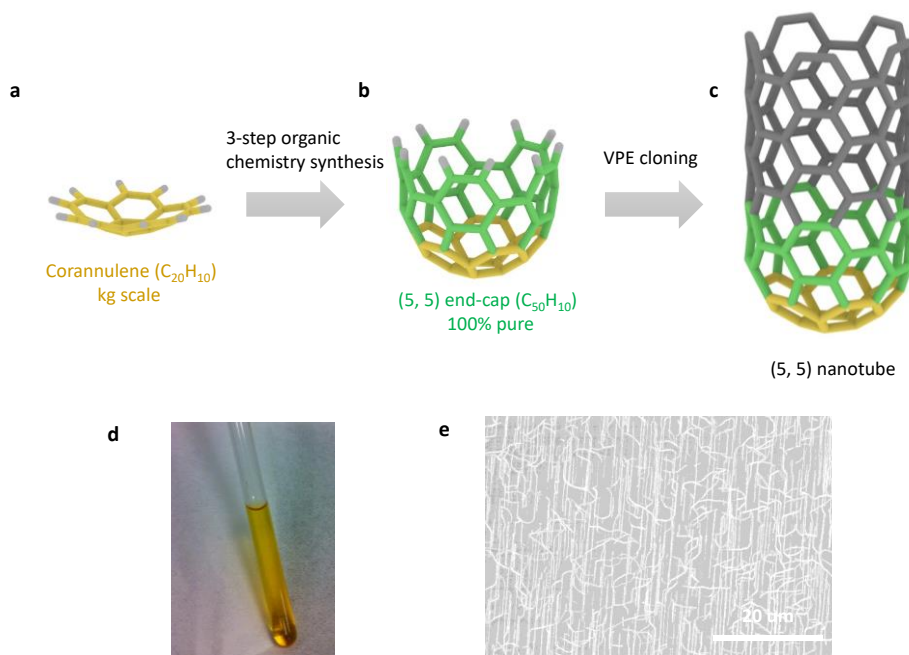


Figure 8. (a) Structure of the bowl-shaped corannulene molecule ($C_{20}H_{10}$) precursor. (b) Structure of the hemispherical $C_{50}H_{10}$ molecule synthesized from corannulene (a), which represents the end-cap plus a short sidewall segment of a (5, 5) SWCNT. The molecule shown in (b) is used for nanotube growth in this study. (c) Structure of a (5, 5) SWCNT. (d) $C_{50}H_{10}$ solution in toluene. (e) A high magnification SEM image of SWCNTs synthesized from $C_{50}H_{10}$ molecules via VPE approach.

We performed systematic Raman spectroscopic analysis with multiple lasers, in order to analyze further the diameter, chirality, and quality of the SWCNTs grown from the pretreated C₅₀H₁₀ molecular end-caps. We found that the C₅₀H₁₀ molecules themselves show very weak Raman signals under short laser wavelength. Fig. 9a–c show representative Raman spectra of as-grown SWCNTs with laser excitation wavelengths of 633 nm (Fig. 9a), 514 nm (Fig. 9b), and 457 nm (Fig. 9c), respectively. The diameters of SWCNTs were deduced from the relationship between the frequencies of radial breathing modes (RBMs) in Raman spectra and nanotube diameters, using the equation $d_t = (223.5/\omega_{\text{RBM}} - 12.5)$. Here, d_t is the diameter of nanotube in nanometer, and ω_{RBM} is the frequency of the RBM in cm⁻¹. We found this equation fits the diameter-RBM relationship in as-grown SWCNTs very well based on our previous studies.²⁶ The peaks marked with arrows are RBMs, while all the other peaks (indicated by asterisks) are from the quartz substrates. In these Raman spectra, most of the RBM peaks are located at wavelengths above 240 cm⁻¹, indicating that small-diameter nanotubes with $d_t < 1$ nm have been grown. Statistical analysis of the RBM frequencies of SWCNTs based on the three laser excitations are shown in Fig. 9e–g, and the diameter distribution of SWCNTs derived from the Raman characterizations are plotted in Fig. 9h, which exhibits an average nanotube diameter of 0.82 nm.

We analyzed the chirality information on the SWCNTs that was obtained by excitation with the three lasers used. Here, we emphasize that for such small-diameter SWCNTs (<1 nm), Raman spectra are unambiguous with respect to chirality assignments, because adjacent SWCNTs have very distinct E_{ii} values and RBM frequencies. Surprisingly, we discovered that most of the nanotubes are actually semiconductors, for example, (8, 3), (6, 1), and (5, 1) in Fig. 9a, (7, 3), and (5, 4) in Fig. 9b, and (8, 1) in Fig. 9c. More interestingly, we observed some RBMs at very high frequencies, for instance, the RBMs at ~ 517 cm⁻¹ are the peaks most frequently observed when using the 633 nm laser (Fig. 9a,e), which corresponds to nanotube diameters of ~ 0.44 nm. We note that only (5, 1) SWCNT should show a RBM peak at this frequency. Therefore, we assign these RBMs to (5, 1) nanotubes. To the best of our knowledge, this is one of the smallest diameter SWCNTs ever reported to have been grown without the necessity of a template confinement.⁵⁰ We point out that the current growth method not only provides a practical way to synthesize such ultra-small-diameter SWCNTs and produces valuable material platforms to allow studies of their exotic properties but also provides critical information on the buildup of the electronic transition energy database of these small nanotubes, which is of fundamental importance to the study of

structure–property relationships of SWCNTs and curvature-induced electronic property changes⁵¹. In addition, the very low defect-induced D-band to tangential G-band intensity ratio (<0.01) suggests a high quality of SWCNTs grown from the pretreated C₅₀H₁₀ molecules (Fig. 9d). Note that the above three lasers are not in resonance with the (5, 5) SWCNTs. We also used a 405 nm laser, which could excite (5, 5) SWCNTs, to characterize our sample. However, we did not observe any RBMs at ~ 340 cm⁻¹ related to (5, 5) nanotubes, indicating no or very small population of (5, 5) chirality in the sample. In fact, when using the 405 nm laser, we observed much fewer RBMs than when using the other three lasers. This is understandable since the 405 nm laser has high energy photons and only very few nanotubes are in resonance with the laser based on the Kataura plot.

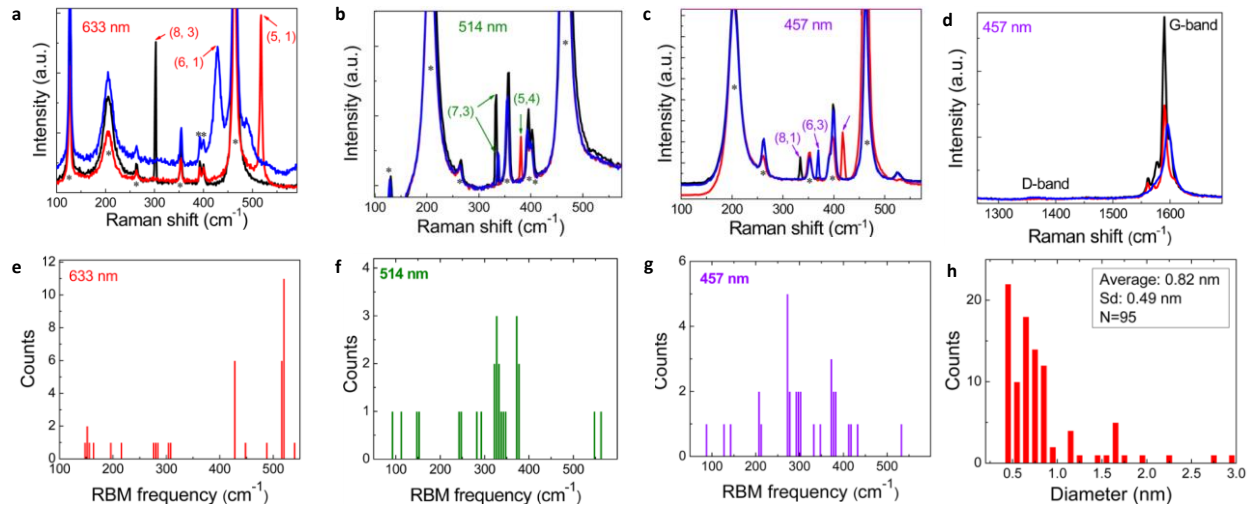


Figure 9. Multiple lasers Raman spectroscopic characterization. (a–c) Raman RBM spectra of SWCNTs grown from C₅₀H₁₀ molecular end-caps excited by 633 nm (a), 514 nm (b), and 457 nm lasers (c). The peaks marked with arrows are from SWCNTs and all the other peaks (marked with *) come from quartz substrates. (d) Raman D-band and G-band spectra of SWCNTs excited by a 457 nm laser. (e–g) RBM frequency distributions based on the above three lasers. (h) Diameter distribution of SWCNTs derived from the RBM frequencies using the equation $d_t = (223.5/\omega_{RBM} - 12.5)$.

Raman spectroscopic characterization points to a trend that nanotubes grown from the pretreated C₅₀H₁₀ may be enriched with semiconducting SWCNTs (Fig. 9). It is difficult, however, to determine the precise metallic/semiconducting ratio of SWCNTs by Raman spectroscopy, owing to their resonant nature. To obtain a quantitative value for the proportion of semiconducting nanotubes rigorously, we performed systematic electrical transport measurements based on individual SWCNT FETs, as well as on aligned array SWCNT FETs combined with the electrical breakdown technique. We first transferred as-grown SWCNTs from quartz to Si/SiO₂ (90 nm

oxide), using a polymer-mediated transfer process,⁵² and fabricated bottom-gate FET devices (Fig. 10a). We have fabricated a total of 13 chips and have tested more than 1000 devices, among which 147 working devices with nanotubes in the channel areas were identified. Among these devices, about 1/4 of them show individual SWCNTs in the channel, while the other 3/4 show parallel SWCNTs forming an array in the channel. Occasionally, a few devices were observed in which no SWCNTs were directly connected to the source and drain electrodes; instead, they formed a random network inside the channel. Such network devices are not included in the following discussion. We plot the distribution of on/off ratios of individual SWCNT FETs (Fig. 10b) and set an on/off ratio criterion of 10 to distinguish metallic SWCNTs from semiconducting ones⁵³⁻⁵⁵. The total number of individual SWCNT FETs is 34, and among them, 32 have on/off ratios larger than 10, giving a semiconducting SWCNT ratio of $32/34 = 94.1\%$. Fig. 10c shows the typical transfer characteristics ($I_{DS}-V_G$) of a semiconducting SWCNT FET (SEM image of the device shown in the inset), which shows p-type behavior with an on/off current ratio of $\sim 3.7 \times 10^4$. As a comparison, Fig. 10d shows the transfer characteristics of another individual SWCNT FET (SEM image shown in the inset) with an on/off ratio of ~ 7 (based on the red curve in Fig. 10d with $V_D = 0.4$ V). Taking into account the evidence from Raman spectroscopic analysis with multiple lasers in Fig. 9 that most of the nanotubes grown from pretreated C₅₀H₁₀ possess rather small diameters, we attribute the curves in Fig. 10d to so-called semimetallic SWCNTs, such as (6, 3) SWCNTs, as detected by Raman characterization in Fig. 9c. Such small-diameter semimetallic SWCNTs have small but finite band gaps between their conduction band and their valence band in the electronic density of states and thus show gate dependence behavior,⁵⁶ as evidenced in Fig. 10d. However, the band gaps of semimetallic SWCNTs are typically very small, for example, ~ 10 meV, which is reflected by the obvious ambipolar transport behavior observed in Fig. 10d. Here we point out that the semimetallic nanotubes with on/off ratio less than 10 (Fig. 10d) are counted as metallic SWCNTs. Actually, we did not observe even a single device with on/off ratio of 1, which would correspond to a true metallic armchair SWCNT.

From SEM observations, we found that a large number of devices contain more than one SWCNT in the channel. For example, the SEM image in the inset of Fig. 10e shows a four-SWCNT array connected to the two electrodes. The transfer characteristic of this device, shown in Fig. 10e, clearly demonstrates the semiconducting behavior with an on/off ratio of ~ 520 for this nanotube-array-FET. We used the electrical breakdown technique⁵⁷ to count the actual number of SWCNTs

for the device in Fig. 10e. As shown in Fig. 10f, we observed a total of three sudden decreases in I_{DS} and, therefore, three SWCNTs being broken during the process. V_D cannot be increased further because the gate oxide will be damaged at V_D of ~ 80 V. We noted that after the breakdown of the third SWCNT at V_D of ~ 70 V, there is still current flow in the channel area, suggesting that at least one more SWCNT is still connected to the electrodes. Taking the SEM image (inset of Fig. 10e) and the breakdown experiments (Fig. 10f) together, we conclude that there were originally a total of four semiconducting SWCNTs in this device, that is, all the visible SWCNTs in the SEM image are indeed connected to both electrodes. This is reasonable, because we first transferred nanotubes and then conducted the electrodes deposition, putting the electrodes on top of the SWCNTs with good contact. Similarly, we have performed systematically electrical breakdown experiments on nanotube-array FETs with on/off ratios < 10 . Fig. 10g shows the transfer curves of such a device before and after electrical breakdown. The blue curve in Fig. 10g shows the initial measurement of the device, which exhibits an on/off ratio of ~ 5 . SEM inspection reveals two SWCNTs connected to both electrodes (inset of Fig. 10g). After the electrical breakdown of the first metallic SWCNT at $V_G = +5$ V (Fig. 10h), the on/off ratio of the device increased to $> 4 \times 10^3$, indicating only one metallic SWCNT in this device. Therefore, we conclude that this device contains one metallic SWCNT and one semiconducting SWCNT. Combining this electrical breakdown and counting technique with SEM imaging, as well as the individual SWCNT FET results, we have identified a total of 264 semiconducting SWCNTs and 8 metallic ones (Table 1), giving a semiconducting SWCNT ratio of $264/272 = 97.1\%$. The error for these statistics is given by equation $\delta = 1.96 \times (\sigma^2/N)^{1/2} = 1.96 \times [p(1 - p)/N]^{1/2} = 2\%$. Here, δ is the statistic error, σ is the standard deviation, N is the number of SWCNTs, p is the semiconducting SWCNT purity, and the confidence coefficient is set as 0.95. We note that this study is not only the very first example of the selective growth of semiconducting SWCNTs by a metal-free process but also stands among one of the highest purity of semiconducting SWCNTs reported so far from a direct growth approach. Such small diameter semiconducting SWCNTs are preferred for short channel transistors because small diameter nanotubes exhibit much smaller OFF state current than large diameter ones.⁵⁸

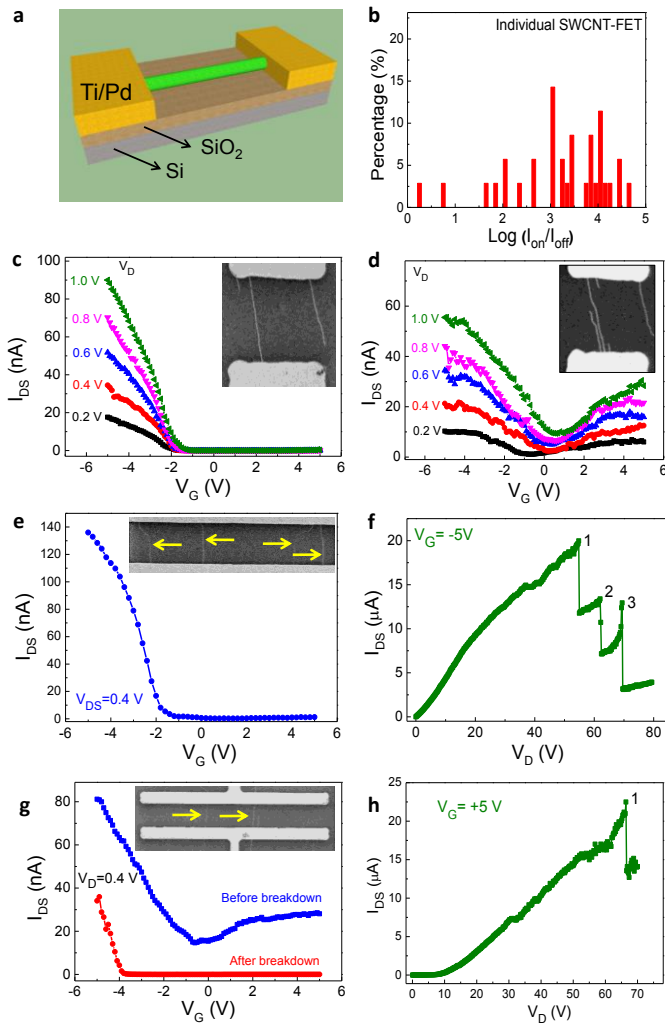


Figure 10. Electrical transport property and breakdown of SWCNT FETs. (a) Schematic of device structure of a back-gated individual SWCNT FET. (b) Statistics of on/off current ratio distribution of 34 individual SWCNT FETs. (c,d) Representative transfer characteristics (I_{DS} - V_G) of an individual semiconducting (c) and semimetallic (d) SWCNT FET with the SEM images of the devices shown in the inset. (e) Transfer characteristic of an all-semiconducting nanotube-array-FET, with the inset SEM image showing a total of four SWCNTs connected to both electrodes. (f) Electrical breakdown experiments of the device in e. (g) Transfer characteristics of a multiple-nanotube-FET before (blue) and after (red) electrical breakdown with the inset SEM image showing a total of two SWCNTs connected to both electrodes. (h) Electrical breakdown experiments of the device in g.

	Total devices	Total SWCNTs	Metallic SWCNTs	Semiconducting SWCNTs
Individual SWCNT FETs	34	34	2	32
SWCNT array FETs	93	238	6	232
All FETs	127	272	8	264
Semiconducting SWCNT ratio = 264/272 = 97.1%				

Table 1. A summary of the total number of SWCNTs from both individual and SWCNT array FETs.

In order to shed light on the underlying mechanism for the chirality mutation during the VPE elongation process of SWCNTs, we further carried out density functional theory (DFT) calculations to study how the chirality of nanotubes evolves during their growth process. Conversion of adjacent hexagon–hexagon (6–6) pairs into pentagon–heptagon (5–7) defects is a potential mechanism by which SWCNT chirality would change, as proposed previously by Smalley and Yakobson.⁵⁹ Each $6-6 \rightarrow 5-7$ conversion changes a $(5, m)$ SWCNT into a structure that could be a template for the succeeding growth of a $(5, m - 1)$ SWCNT. DFT calculations (Fig. 11a) indicate a prohibitive barrier impedes this pathway for pristine $C_{50}H_{10}$ molecule. However, the barrier for $6-6 \rightarrow 5-7$ conversion reduces by a factor of 3 for dehydrogenated $C_{50}H_{10}$ molecules, that is, from 171.0 kcal/mol (for $C_{50}H_{10}$) to 62.8 kcal/mol (for $C_{50}H_9$, which is the dehydrogenated $C_{50}H_{10}$). Fig. 11b,c depicts the structures of the transition states (TS) for both cases. Because oxygen and water were used during seed pretreatment, it is possible that this could result in dehydrogenation of $C_{50}H_{10}$ or creation of some other active radical species that would have similar low barriers for $6-6 \rightarrow 5-7$ conversion. Such active species would promote a greater extent of chirality change during nanotube growth. In a similar manner, consecutive $6-6 \rightarrow 5-7$ conversions can take place from the intermediates (or templates) for growth of other $(5, m)$ SWCNTs ($m=3, 2, 1$) (Figure 6d–f).⁵⁹ DFT calculations further show that these processes are promoted when the $6-6 \rightarrow 5-7$ conversion takes place adjacent to the pentagon of an existing 5–7 defect, producing templates for the growth of $(5, m - 1)$ SWCNTs. The barriers for these successive transformations are lower than that of the initial $(5, 5) \rightarrow (5, 4)$ transformation, and reduce slightly in the order: $(5, 3) \rightarrow (5, 2) > (5, 1) \rightarrow (5, 0) > (5, 2) \rightarrow (5, 1) > (5, 4) \rightarrow (5, 3)$ (Fig. 11d). The trend is the same for high temperatures of 1173 and 298.15 K. The possibility of such transformations to occur can be described as the exponential factor $-(E_b/kT)$, where E_b is the activation free energy, k is the Boltzmann constant, and T is the temperature. At 1173 K (i.e., the nanotube growth temperature used in this study), an energy barrier of $E_b = 60.8$ kcal/mol is not very high, suggesting that these steps are not prohibitive for the dehydrogenated species. With more active intermediates, this possibility could be even larger. In certain degree, these theoretical results reveal the changes of nanotube chirality after growth process. However, the theoretical results cannot explain why there are no $(5, 5)$ SWCNTs grown in the products. The lack of $(5, 5)$ SWCNTs is still very puzzling to us at this stage, which needs further study. In addition, based on

Raman analysis in Fig. 9, we observed that some nanotubes have diameters larger than the $C_{50}H_{10}$ molecules, for example, (8, 3). These nanotubes presumably originate from the aggregation of a few molecules into relatively large structures and consequently, nanotubes with diameters larger than (5, 5) were grown.

Previous DFT calculations suggest that structure-dependent stability differences of metallic versus semiconducting SWCNTs are much more significant in the small diameter regime than in medium or large diameter regime.⁶⁰ As nanotubes grown from pretreated $C_{50}H_{10}$ end-caps possess exceptionally small diameters, we speculate that nanotube diameter-induced stability differences between metallic and semiconducting SWCNTs, which may play a central role at the very small diameter regime, might be the key reason for the preferential growth of semiconducting SWCNTs in this study. The nucleation and growth of such small diameter SWCNTs on flat substrates may relate to the special molecular seeds used here, which serve as nanotube end-caps and stabilize nuclei of very small diameter nanotubes.

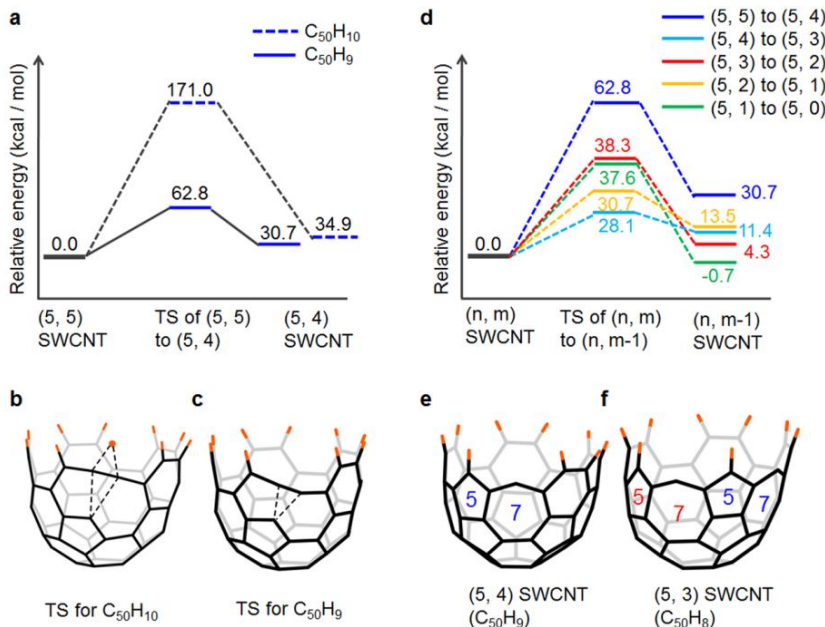


Figure 11. DFT calculations of the energy profiles of the $(5, m) \rightarrow (5, m-1)$ chirality transformations and the structures of the transition states (TS). (a) Energy barriers of $(5, 5) \rightarrow (5, 4)$ transformation for $C_{50}H_{10}$ and $C_{50}H_9$. (b,c) Structures of TS of the $(5, 5) \rightarrow (5, 4)$ transformation starting from $C_{50}H_{10}$ and $C_{50}H_9$, respectively. (d) Energy barriers of $(5, m) \rightarrow (5, m-1)$ transformations for $m = 5, 4, 3, 2$, and 1, starting from $C_{50}H_{m+4}$. (e,f) Structures of the formed (5, 4) and (5, 3) chirality, with one and two adjacent 5-7 pairs, respectively. The calculated energy includes the zero point vibration energy (ZPVE).

To conclude, in this section of the report, we show our results of using a nanotube-end-cap molecule, C₅₀H₁₀, prepared by bottom-up organic chemistry synthesis, for the first time to grow SWCNTs having nearly pure semiconducting properties via metal-free VPE cloning approach. This study not only establishes an efficient approach to grow nearly pure SWCNT semiconductors but also provides valuable new insight into the selective growth mechanism of SWCNTs.

Summary

In summary, we successfully demonstrated a novel and robust approach, vapor-phase epitaxy, for producing nanotubes of predefined chirality, by combining nanotube separation with CVD synthesis. Then, we further carried out systematic investigations of the chirality-dependent growth kinetics and termination mechanism for the vapor-phase epitaxial growth of seven single-chirality nanotubes of (9, 1), (6, 5), (8, 3), (7, 6), (10, 2), (6, 6), and (7, 7), covering near zigzag, medium chiral angle, and near armchair semiconductors, as well as armchair metallic nanotubes. Furthermore, we explored and successfully managed to elongate organic synthesized (5, 5) end-cap molecules into small-diameter nearly pure semiconducting SWCNTs with VPE cloning approach. All the results presented in this report not only demonstrated a highly robust strategy, VPE cloning approach, to achieve chirality-predefined synthesis of SWCNTs, but also deepen our understanding of the chirality-dependent SWCNT growth kinetics and the underlying mechanism.

Reference

1. Tans, S. J.; Devoret, M. H.; Dai, H. J.; Thess, A.; Smalley, R. E.; Geerligs, L. J.; Dekker, C., Individual single-wall carbon nanotubes as quantum wires. *Nature* 1997, 386, 474-477.
2. Chernozatonskii, L., Three-terminal junctions of carbon nanotubes: synthesis, structures, properties and applications. *J Nanopart Res* 2003, 5, 473-484.
3. Bockrath, M.; Cobden, D. H.; McEuen, P. L.; Chopra, N. G.; Zettl, A.; Thess, A.; Smalley, R. E., Single-electron transport in ropes of carbon nanotubes. *Science* 1997, 275, 1922-1925.
4. Tans, S. J.; Verschueren, A. R. M.; Dekker, C., Room-temperature transistor based on a single carbon nanotube. *Nature* 1998, 393, 49-52.
5. Javey, A.; Guo, J.; Wang, Q.; Lundstrom, M.; Dai, H. J., Ballistic carbon nanotube field-effect transistors. *Nature* 2003, 424, 654-657.
6. Chen, Z. H.; Appenzeller, J.; Lin, Y. M.; Sippel-Oakley, J.; Rinzler, A. G.; Tang, J. Y.; Wind, S. J.; Solomon, P. M.; Avouris, P., An integrated logic circuit assembled on a single carbon nanotube. *Science* 2006, 311, 1735-1735.
7. Kang, S. J.; Kocabas, C.; Ozel, T.; Shim, M.; Pimparkar, N.; Alam, M. A.; Rotkin, S. V.; Rogers, J. A., High-performance electronics using dense, perfectly aligned arrays of single-walled carbon nanotubes. *Nat Nanotechnol* 2007, 2, 230-236.

8. Sun, D. M.; Timmermans, M. Y.; Tian, Y.; Nasibulin, A. G.; Kauppinen, E. I.; Kishimoto, S.; Mizutani, T.; Ohno, Y., Flexible high-performance carbon nanotube integrated circuits. *Nat Nanotechnol* 2011, 6, 156-161.

9. Ryu, K.; Badmaev, A.; Wang, C.; Lin, A.; Patil, N.; Gomez, L.; Kumar, A.; Mitra, S.; Wong, H. S. P.; Zhou, C. W., CMOS-Analogous Wafer-Scale Nanotube-on-Insulator Approach for Submicrometer Devices and Integrated Circuits Using Aligned Nanotubes. *Nano Lett* 2009, 9, 189-197.

10. Liu, Z.; Tabakman, S.; Welsher, K.; Dai, H. J., Carbon Nanotubes in Biology and Medicine: In vitro and in vivo Detection, Imaging and Drug Delivery. *Nano Res* 2009, 2, 85-120.

11. Liu, H. P.; Nishide, D.; Tanaka, T.; Kataura, H., Large-scale single-chirality separation of single-wall carbon nanotubes by simple gel chromatography. *Nat Commun* 2011, 2.

12. Tu, X. M.; Manohar, S.; Jagota, A.; Zheng, M., DNA sequence motifs for structure-specific recognition and separation of carbon nanotubes. *Nature* 2009, 460, 250-253.

13. Green, A. A.; Hersam, M. C., Nearly Single-Chirality Single-Walled Carbon Nanotubes Produced via Orthogonal Iterative Density Gradient Ultracentrifugation. *Adv Mater* 2011, 23, 2185-+.

14. Ghosh, S.; Bachilo, S. M.; Weisman, R. B., Advanced sorting of single-walled carbon nanotubes by nonlinear density-gradient ultracentrifugation. *Nat Nanotechnol* 2010, 5, 443-450.

15. Krupke, R.; Hennrich, F.; von Lohneysen, H.; Kappes, M. M., Separation of metallic from semiconducting single-walled carbon nanotubes. *Science* 2003, 301, 344-347.

16. Li, Y. M.; Mann, D.; Rolandi, M.; Kim, W.; Ural, A.; Hung, S.; Javey, A.; Cao, J.; Wang, D. W.; Yenilmez, E.; Wang, Q.; Gibbons, J. F.; Nishi, Y.; Dai, H. J., Preferential growth of semiconducting single-walled carbon nanotubes by a plasma enhanced CVD method. *Nano Lett* 2004, 4, 317-321.

17. Harutyunyan, A. R.; Chen, G. G.; Paronyan, T. M.; Pigos, E. M.; Kuznetsov, O. A.; Hewaparakrama, K.; Kim, S. M.; Zakharov, D.; Stach, E. A.; Sumanasekera, G. U., Preferential Growth of Single-Walled Carbon Nanotubes with Metallic Conductivity. *Science* 2009, 326, 116-120.

18. Ding, L.; Tselev, A.; Wang, J. Y.; Yuan, D. N.; Chu, H. B.; McNicholas, T. P.; Li, Y.; Liu, J., Selective Growth of Well-Aligned Semiconducting Single-Walled Carbon Nanotubes. *Nano Lett* 2009, 9, 800-805.

19. Engel, M.; Small, J. P.; Steiner, M.; Freitag, M.; Green, A. A.; Hersam, M. C.; Avouris, P., Thin Film Nanotube Transistors Based on Self-Assembled, Aligned, Semiconducting Carbon Nanotube Arrays. *AcS Nano* 2008, 2, 2445-2452.

20. Wang, C.; Zhang, J. L.; Ryu, K. M.; Badmaev, A.; De Arco, L. G.; Zhou, C. W., Wafer-Scale Fabrication of Separated Carbon Nanotube Thin-Film Transistors for Display Applications. *Nano Lett* 2009, 9, 4285-4291.

21. Ryu, K. M.; Badmaev, A.; Gomez, L.; Ishikawa, F.; Lei, B.; Zhou, C. W., Synthesis of aligned single-walled nanotubes using catalysts defined by nanosphere lithography. *J Am Chem Soc* 2007, 129, 10104-+.

22. Smalley, R. E.; Li, Y. B.; Moore, V. C.; Price, B. K.; Colorado, R.; Schmidt, H. K.; Hauge, R. H.; Barron, A. R.; Tour, J. M., Single wall carbon nanotube amplification: En route to a type-specific growth mechanism. *J Am Chem Soc* 2006, 128, 15824-15829.

23. Wang, Y. H.; Kim, M. J.; Shan, H. W.; Kittrell, C.; Fan, H.; Ericson, L. M.; Hwang, W. F.; Arepalli, S.; Hauge, R. H.; Smalley, R. E., Continued growth of single-walled carbon nanotubes. *Nano Lett* 2005, 5, 997-1002.

24. Yao, Y. G.; Feng, C. Q.; Zhang, J.; Liu, Z. F., "Cloning" of Single-Walled Carbon Nanotubes via Open-End Growth Mechanism. *Nano Lett* 2009, 9, 1673-1677.

25. Liu, J.; Wang, C.; Tu, X. M.; Liu, B. L.; Chen, L.; Zheng, M.; Zhou, C. W., Chirality-controlled synthesis of single-wall carbon nanotubes using vapour-phase epitaxy. *Nat Commun* 2012, 3.

26. Liu, B. L.; Liu, J.; Tu, X. M.; Zhang, J. L.; Zheng, M.; Zhou, C. W., Chirality-Dependent Vapor-Phase Epitaxial Growth and Termination of Single-Wall Carbon Nanotubes. *Nano Lett* 2013, 13, 4416-4421.

27. Liu, B. L.; Liu, J.; Li, H. B.; Bhola, R.; Jackson, E. A.; Scott, L. T.; Page, A.; Irle, S.; Morokuma, K.; Zhou, C. W., Nearly Exclusive Growth of Small Diameter Semiconducting Single-Wall Carbon Nanotubes from Organic Chemistry Synthetic End-Cap Molecules. *Nano Lett* 2015, 15, 586-595.

28. Hersam, M. C., Progress towards monodisperse single-walled carbon nanotubes. *Nat Nanotechnol* 2008, 3, 387-394.

29. Tu, X. M.; Walker, A. R. H.; Khrapin, C. Y.; Zheng, M., Evolution of DNA Sequences Toward Recognition of Metallic Armchair Carbon Nanotubes. *J Am Chem Soc* 2011, 133, 12998-13001.

30. Xiao, J. L.; Dunham, S.; Liu, P.; Zhang, Y. W.; Kocabas, C.; Moh, L.; Huang, Y. G.; Hwang, K. C.; Lu, C.; Huang, W.; Rogers, J. A., Alignment Controlled Growth of Single-Walled Carbon Nanotubes on Quartz Substrates. *Nano Lett* 2009, 9, 4311-4319.

31. Fantini, C.; Jorio, A.; Souza, M.; Strano, M. S.; Dresselhaus, M. S.; Pimenta, M. A., Optical transition energies for carbon nanotubes from resonant Raman spectroscopy: Environment and temperature effects. *Phys Rev Lett* 2004, 93.

32. Fantini, C.; Jorio, A.; Santos, A. P.; Peressinotto, V. S. T.; Pimenta, M. A., Characterization of DNA-wrapped carbon nanotubes by resonance Raman and optical absorption spectroscopies. *Chem Phys Lett* 2007, 439, 138-142.

33. Fort, E. H.; Donovan, P. M.; Scott, L. T., Diels-Alder Reactivity of Polycyclic Aromatic Hydrocarbon Bay Regions: Implications for Metal-Free Growth of Single-Chirality Carbon Nanotubes. *J Am Chem Soc* 2009, 131, 16006-+.

34. Fort, E. H.; Jeffreys, M. S.; Scott, L. T., Diels-Alder cycloaddition of acetylene gas to a polycyclic aromatic hydrocarbon bay region. *Chem Commun* 2012, 48, 8102-8104.

35. Kato, T.; Hatakeyama, R., Direct Growth of Short Single-Walled Carbon Nanotubes with Narrow-Chirality Distribution by Time-Programmed Plasma Chemical Vapor Deposition. *Acs Nano* 2010, 4, 7395-7400.

36. Lu, C. G.; Liu, J., Controlling the diameter of carbon nanotubes in chemical vapor deposition method by carbon feeding. *J Phys Chem B* 2006, 110, 20254-20257.

37. Rao, R.; Liptak, D.; Cherukuri, T.; Yakobson, B. I.; Maruyama, B., In situ evidence for chirality-dependent growth rates of individual carbon nanotubes. *Nat Mater* 2012, 11, 213-216.

38. Li, H. B.; Page, A. J.; Irle, S.; Morokuma, K., Single-walled Carbon Nanotube Growth from Chiral Carbon Nanorings: Prediction of Chirality and Diameter Influence on Growth Rates. *J Am Chem Soc* 2012, 134, 15887-15896.

39. Khan, M. S.; Crynes, B. L., Survey Of Recent Methane Pyrolysis Literature - a Survey Of Methane Pyrolysis Data Is Presented And Discussed. *Ind Eng Chem* 1970, 62, 54-8.

40. Abanades, S.; Flamant, G., Production of hydrogen by thermal methane splitting in a nozzle-type laboratory-scale solar reactor. *Int J Hydrogen Energ* 2005, 30, 843-853.

41. Li, H. B.; Page, A. J.; Irle, S.; Morokuma, K., Theoretical Insights into Chirality-Controlled SWCNT Growth from a Cycloparaphenylen Template. *Chemphyschem* 2012, 13, 1479-1485.

42. Bierman, M. J.; Lau, Y. K. A.; Kvit, A. V.; Schmitt, A. L.; Jin, S., Dislocation-driven nanowire growth and Eshelby twist. *Science* 2008, 320, 1060-1063.

43. Nanot, S.; Haroz, E. H.; Kim, J. H.; Hauge, R. H.; Kono, J., Optoelectronic Properties of Single-Wall Carbon Nanotubes. *Adv Mater* 2012, 24, 4977-4994.

44. Zhu, Z.; Jiang, H.; Susi, T.; Nasibulin, A. G.; Kauppinen, E. I., The Use of NH₃ to Promote the Production of Large-Diameter Single-Walled Carbon Nanotubes with a Narrow (n,m) Distribution. *J Am Chem Soc* 2011, 133, 1224-1227.

45. Hitosugi, S.; Nakanishi, W.; Yamasaki, T.; Isobe, H., Bottom-up synthesis of finite models of helical (n,m)-single-wall carbon nanotubes. *Nat Commun* 2011, 2.

46. Scott, L. T.; Jackson, E. A.; Zhang, Q. Y.; Steinberg, B. D.; Bancu, M.; Li, B., A Short, Rigid, Structurally Pure Carbon Nanotube by Stepwise Chemical Synthesis. *J Am Chem Soc* 2012, 134, 107-110.

47. Yagi, A.; Segawa, Y.; Itami, K., Synthesis and Properties of [9]Cyclo-1,4-naphthylene: A pi-Extended Carbon Nanoring. *J Am Chem Soc* 2012, 134, 2962-2965.

48. Jasti, R.; Bhattacharjee, J.; Neaton, J. B.; Bertozi, C. R., Synthesis, Characterization, and Theory of [9]-, [12]-, and [18]Cycloparaphenylenes: Carbon Nano hoop Structures. *J Am Chem Soc* 2008, 130, 17646-+.

49. Sanchez-Valencia, J. R.; Dienel, T.; Groning, O.; Shorubalko, I.; Mueller, A.; Jansen, M.; Amsharov, K.; Ruffieux, P.; Fasel, R., Controlled synthesis of single-chirality carbon nanotubes. *Nature* 2014, 512, 61-+.

50. Tang, Z. K.; Zhai, J. P.; Tong, Y. Y.; Hu, X. J.; Saito, R.; Feng, Y. J.; Sheng, P., Resonant Raman scattering of the smallest single-walled carbon nanotubes. *Phys Rev Lett* 2008, 101.

51. Salvetat, J. P.; Bonard, J. M.; Bacsa, R.; Stockli, T.; Forro, L., Physical properties of carbon nanotubes. *Electronic Properties Of Novel Materials - Progress In Molecular Nanostructures* 1998, 442, 467-480.

52. Liu, B. L.; Ren, W. C.; Gao, L. B.; Li, S. S.; Pei, S. F.; Liu, C.; Jiang, C. B.; Cheng, H. M., Metal-Catalyst-Free Growth of Single-Walled Carbon Nanotubes. *J Am Chem Soc* 2009, 131, 2082-+.

53. Che, Y. C.; Wang, C.; Liu, J.; Liu, B. L.; Lin, X.; Parker, J.; Beasley, C.; Wong, H. S. P.; Zhou, C. W., Selective Synthesis and Device Applications of Semiconducting Single-Walled Carbon Nanotubes Using Isopropyl Alcohol as Feedstock. *Acs Nano* 2012, 6, 7454-7462.

54. Hong, G.; Zhang, B.; Peng, B. H.; Zhang, J.; Choi, W. M.; Choi, J. Y.; Kim, J. M.; Liu, Z. F., Direct Growth of Semiconducting Single-Walled Carbon Nanotube Array. *J Am Chem Soc* 2009, 131, 14642-+.

55. Zhang, G. Y.; Qi, P. F.; Wang, X. R.; Lu, Y. R.; Li, X. L.; Tu, R.; Bangsaruntip, S.; Mann, D.; Zhang, L.; Dai, H. J., Selective etching of metallic carbon nanotubes by gas-phase reaction. *Science* 2006, 314, 974-977.

56. Zhou, C. W.; Kong, J.; Dai, H. J., Intrinsic electrical properties of individual single-walled carbon nanotubes with small band gaps. *Phys Rev Lett* 2000, 84, 5604-5607.

57. Collins, P. C.; Arnold, M. S.; Avouris, P., Engineering carbon nanotubes and nanotube circuits using electrical breakdown. *Science* 2001, 292, 706-709.

58. Seidel, R. V.; Graham, A. P.; Kretz, J.; Rajasekharan, B.; Duesberg, G. S.; Liebau, M.; Unger, E.; Kreupl, F.; Hoenlein, W., Sub-20 nm short channel carbon nanotube transistors. *Nano Lett* 2005, 5, 147-150.

59. Smalley, R. E.; Yakobson, B. I., The future of the fullerenes. *Solid State Commun* 1998, 107, 597-606.

60. Li, Y. M.; Peng, S.; Mann, D.; Cao, J.; Tu, R.; Cho, K. J.; Dai, H. J., On the origin of preferential growth of semiconducting single-walled carbon nanotubes. *J Phys Chem B* 2005, 109, 6968-6971.

AFOSR Deliverables Submission Survey

Response ID:6861 Data

1.

Report Type

Final Report

Primary Contact Email

Contact email if there is a problem with the report.

chongwuz@usc.edu

Primary Contact Phone Number

Contact phone number if there is a problem with the report

213-740-4708

Organization / Institution name

University of Southern California

Grant/Contract Title

The full title of the funded effort.

Chirality-controlled growth of single-wall carbon nanotubes using vapor phase epitaxy: mechanistic understanding and scalable production

Grant/Contract Number

AFOSR assigned control number. It must begin with "FA9550" or "F49620" or "FA2386".

FA9550-14-1-0115

Principal Investigator Name

The full name of the principal investigator on the grant or contract.

Zhou, Chongwu Zheng, Ming

Program Officer

The AFOSR Program Officer currently assigned to the award

Lee, Charles

Reporting Period Start Date

06/14/2014

Reporting Period End Date

06/14/2016

Abstract

In this report, we present our efforts in establishing a novel and effective approach for chirality-controlled synthesis of single-wall carbon nanotubes. Firstly, we have successfully demonstrated a vapor-phase-epitaxy-analogous general strategy for producing nanotubes of predefined chirality. By combining nanotube separation with synthesis, we have achieved controlled growth of nanotubes with preselected chirality. Moreover, we carried out systematic investigations of the chirality-dependent growth kinetics and termination mechanism for the vapor-phase epitaxial growth of seven different single-chirality nanotubes of (9, 1), (6, 5), (8, 3), (7, 6), (10, 2), (6, 6), and (7, 7), covering near zigzag, medium chiral angle, and near armchair semiconductors, as well as armchair metallic nanotubes. Furthermore, we explored and successfully managed to elongate organic synthesized (5, 5) end-cap molecules into small-diameter nearly-pure-semiconducting single-wall carbon nanotubes with vapor-phase-epitaxy cloning approach.

Distribution Statement

This is block 12 on the SF298 form.

Distribution A - Approved for Public Release. Distribution A. Distribution approved for public release.

Explanation for Distribution Statement

If this is not approved for public release, please provide a short explanation. E.g., contains proprietary information.

SF298 Form

Please attach your [SF298](#) form. A blank SF298 can be found [here](#). Please do not password protect or secure the PDF

The maximum file size for an SF298 is 50MB.

[SF298.pdf](#)

Upload the Report Document. File must be a PDF. Please do not password protect or secure the PDF . The maximum file size for the Report Document is 50MB.

[Final Report.pdf](#)

Upload a Report Document, if any. The maximum file size for the Report Document is 50MB.

Archival Publications (published) during reporting period:

[1] Liu, J.; Wang, C.; Tu, X. M.; Liu, B. L.; Chen, L.; Zheng, M.; Zhou, C. W., Chirality-controlled synthesis of single-wall carbon nanotubes using vapour-phase epitaxy. *Nat Commun* 2012, 3.

[2] Liu, B. L.; Liu, J.; Tu, X. M.; Zhang, J. L.; Zheng, M.; Zhou, C. W., Chirality-Dependent Vapor-Phase Epitaxial Growth and Termination of Single-Wall Carbon Nanotubes. *Nano Lett* 2013, 13, 4416-4421.

[3] Liu, B. L.; Liu, J.; Li, H. B.; Bhola, R.; Jackson, E. A.; Scott, L. T.; Page, A.; Irle, S.; Morokuma, K.; Zhou, C. W., Nearly Exclusive Growth of Small Diameter Semiconducting Single-Wall Carbon Nanotubes from Organic Chemistry Synthetic End-Cap Molecules. *Nano Lett* 2015, 15, 586-595.

New discoveries, inventions, or patent disclosures:

Do you have any discoveries, inventions, or patent disclosures to report for this period?

No

Please describe and include any notable dates

Do you plan to pursue a claim for personal or organizational intellectual property?

Changes in research objectives (if any):

Change in AFOSR Program Officer, if any:

Extensions granted or milestones slipped, if any:

AFOSR LRIR Number

LRIR Title

Reporting Period

Laboratory Task Manager

Program Officer

Research Objectives

Technical Summary

Funding Summary by Cost Category (by FY, \$K)

	Starting FY	FY+1	FY+2
Salary			
Equipment/Facilities			
Supplies			
Total			

Report Document

Report Document - Text Analysis

Report Document - Text Analysis

Appendix Documents

2. Thank You

E-mail user

Sep 12, 2016 20:16:27 Success: Email Sent to: chongwuz@usc.edu